American Mineralogist, Volume 94, pages 616–621, 2009

High-pressure phase transformation in $LiFeGe_2O_6$ pyroxene

Fabrizio Nestola,[1,*] Günther J. Redhammer,[2] Martha G. Pamato,[1] Luciano Secco,[1] and Alberto Dal Negro[1]

[1]Dipartimento di Geoscienze, Università di Padova, Via Giotto 1, I-35135 Padova, Italy
[2]Department of Materials Engineering and Physics, Division of Mineralogy, University of Salzburg, Hellbrunnerstr, 34, 24 A-5020 Salzburg, Austria

Abstract

A synthetic pyroxene with composition $LiFeGe_2O_6$ and space group $P2_1/c$ at ambient conditions was investigated by single-crystal X-ray diffraction using a diamond anvil cell. The unit-cell parameters and crystal structure were determined at eight different pressures up to 8.7 GPa. Between 4.16 and 4.83 GPa, the sample shows a strongly first-order phase transition as indicated by a drastic drop in *a*, *c*, β, and unit-cell volume. The transition is marked by the disappearance of *b*-type reflections ($h + k$ = odd) forbidden in a *C*-centered lattice. The volume bulk modulus of the $P2_1/c$ phase is estimated to be 110 GPa as compared to 147 GPa of the $C2/c$ one. The crystal structure evolution as a function of pressure is mainly influenced by the kinking of tetrahedral chains; the A and B non-symmetry equivalent chains of the $P2_1/c$ phase undergo strong deformations up to 4.16 GPa (A chain ~2%, B chain ~5.3%). At the transition, the two chains become symmetry equivalent and the single tetrahedral chain of the $C2/c$ phase shows only minor deformations with pressure (~1.9%) due to its already strong kinking (~130°). Such behavior is the main reason for the strong difference in compressibility between the low- and high-symmetry forms.

Keywords: Single-crystal structure analysis, germanates, high-pressure phase transformations, X-ray diffraction

Introduction

Li-bearing silicate pyroxenes have been recently investigated at high pressure as such phases undergo a $C2/c$–$P2_1/c$ phase transition (e.g., $LiAlSi_2O_6$, $LiGaSi_2O_6$, $LiScSi_2O_6$, $LiFeSi_2O_6$: Arlt and Angel 2000; Pommier et al. 2005; Nestola et al. 2008) similar to that observed in clinopyroxenes stable at Earth's mantle conditions [e.g., $(Mg,Ca,Fe)SiO_3$: Angel et al. 1992; Nestola et al. 2004]. Previous works provided topological models capable of predicting the behavior of pyroxene as a function of pressure, temperature, and composition (Downs 2003; Thompson and Downs 2003). An important difference between Li-bearing and mantle clinopyroxenes concerns the $C2/c$ phases involved in the transformation. Generally, mantle clinopyroxenes showing this transition are $P2_1/c$ at room pressure and transform to $C2/c$ at high pressure, whereas Li-bearing clinopyroxenes are $C2/c$ at room pressure and become $P2_1/c$ at high pressure. One exception is the composition $Li_{0.85}Mg_{0.09}Fe^{2+}_{0.06}Fe^{3+}_{0.85}Mg_{0.15}Si_2O_6$, which maintains the $P2_1/c$ symmetry from ambient conditions up to at least 8 GPa (Gatta et al. 2005).

The $C2/c$ high-pressure phase of mantle clinopyroxenes is structurally distinct from the low-pressure phase typical for Li-bearing clinopyroxenes. It is characterized by a strongly kinked tetrahedral chain. Such structures are denoted as HP$C2/c$ and show kinking angles close to 140° (e.g., $Mg_{1.85}Ca_{0.15}Si_2O_6$, Nestola et al. 2004), whereas the low-pressure $C2/c$ phase is denoted as HT$C2/c$ and shows a much more extended tetrahedral chain [e.g., 170° for $LiAlSi_2O_6$ (Arlt and Angel 2000); 179.9° in $LiGaSi_2O_6$ (Redhammer and Roth 2004); 180.8° in $LiFeSi_2O_6$ (Redhammer et al. 2001)]. To our best knowledge, there is just one published report on the high-pressure crystal structure evolution of the HP$C2/c$ phase, focused on composition $Fe_2Ge_2O_6$ (tetrahedral chain kinking angle at room pressure = 131.1°: Hattori et al. 2000). Considering that the HP$C2/c$ structure should be the stable one at Earth's mantle conditions, it is important to perform systematic studies to better constrain the behavior of such phases. Moreover, as it is well known that many germanates show phase transformations similar to those of silicates, but at lower pressures (Ross and Navrotsky 1988), germanate clinopyroxenes can be used as structural models for investigating the behavior of mantle clinopyroxenes (e.g., clinoenstatite $Mg_2Si_2O_6$). In this work, we synthesized and studied by single-crystal X-ray diffraction in situ at high pressure a sample with composition $LiFeGe_2O_6$. This composition was chosen because the complete substitution of Si by Ge and Li for Fe stabilizes the $P2_1/c$ symmetry at room pressure, which enables us to also characterize the $P2_1/c$–HP$C2/c$ phase transition and the crystal structure evolution of the HP$C2/c$ phase.

* E-mail: fabrizio.nestola@unipd.it

EXPERIMENTAL METHODS

Single crystals with nominal composition $LiFeGe_2O_6$ were synthesized by the high-temperature solution (flux-growth) technique using a mixture of 80 mol% Li_2MoO_4 and 20 mol% $LiVO_3$ as a solvent. A flux to nutrient ratio of 10:1 was chosen. The finely ground, homogeneous mixture of Li_2CO_3, Fe_2O_3, and GeO_2 with the stoichiometry of $LiFeGe_2O_6$, together with the flux, was put into a platinum crucible, covered with a lid, and heated in a chamber furnace to 1473 K, held for 24 h at 1473 K and cooled to 1073 K at a rate of 2 K/h. After soaking the flux with hot distilled water large pale green needle-like to short prismatic single crystals of $LiFeGe_2O_6$ up to 3 mm in size were obtained.

A crystal 200 × 50 × 50 μm in size, optically free of twinning and defects, and characterized by sharp optical extinction, was chosen for the in situ study by high-pressure X-ray diffraction using a diamond anvil cell (DAC). The crystal was loaded in an ETH-type DAC using anvil diamonds with standard geometry (height 1.4 mm, table 2.8 mm, girdle 3.0 mm) and culets 600 μm in diameter, with T301 steel gaskets preindented to 90 μm and with a hole 250 μm in diameter. A 16:3:1 methanol:ethanol:water mixture was used as a pressure-transmitting medium that behaves hydrostatically to the highest pressures reached in this work (Angel et al. 2007). Ruby spheres were included as internal pressure markers (Mao et al. 1986).

Unit-cell parameters and full intensity data sets were collected at eight different pressures to 8.7 GPa on a STOE STADI4 four-circle diffractometer (monochromatized Mo$K\alpha$ radiation) equipped with an Oxford Diffraction CCD detector. Data were collected to $2\theta_{max} = 60°$ using an exposure time of 60 s and an ω-scan of 0.2° to improve the accuracy and precision of the unit-cell parameters. The sample-detector distance was 60 mm. The CrysAlis RED program (Oxford Diffraction) was used to integrate the intensity data, applying the Lorentz-polarization correction. The absorption correction for crystal, DAC, and gasket shadowing was performed using Absorb 6.0 (Angel 2004). Weighted isotropic structure refinements (only Fe and Ge were refined anisotropically) were done using the SHELX-97 package (Sheldrick 1997) in space group $P2_1/c$ at room pressure using the coordinates of pigeonite as a starting model (Nestola et al. 2004). Note that the space group was also confirmed by the presence of *b*-type reflections ($h + k$ = odd) typical of a primitive lattice. The crystal data and structure refinements are reported in Table 1, atomic coordinates and displacement parameters are reported in Table 2, and selected bond lengths, polyhedral volumes, distortion of polyhedral geometry and angles are reported in Table 3. The room pressure crystal structure of $LiFeGe_2O_6$ was refined with the crystal both in air and in the DAC. The CIF[1] file shows excellent agreement between the atomic coordinates of the two structures.

RESULTS

Phase transition and elasticity

In Figure 1, the evolution of *a*, *b*, *c*, β, and *V* is shown as a function of pressure. From Figure 1a, it is obvious that the *a*, *b*, and *c* parameters decrease with pressure and that, whereas *a* and *c* show a strong discontinuity between 4.1 and 4.8 GPa, the *b* parameter decreases continuously to the maximum pressure reached. The total decrease from room pressure to 8.7 GPa is 5.2, 2.3, and 6.0% for *a*, *b*, and *c*, respectively. The β angle, as found for *a* and *c*, shows a drastic drop from 108.49 to 101.55° between 4.1 and 4.8 GPa (Fig. 1b), with a decrease of about 6.8%. As a consequence of the evolution of *a*, *c*, and β, the unit-cell volume *V* decreases with pressure, showing a marked drop between 4.1 and 4.8 GPa (Fig. 1c), accompanied by a negative variation by about 3% and a total negative variation between room pressure and 8.7 GPa of about 10%. The discontinuity is accompanied by the sudden disappearance of the *b*-type reflections. Analysis of the complete intensity data collected at each pressure, at which the unit-cell parameters were determined, clearly indicates a phase transformation from $P2_1/c$ to $C2/c$. As will be explained in the next paragraph, the transition is the same as found for the mantle clinopyroxenes, i.e., $P2_1/c$ to HP$C2/c$ (tetrahedral chain kinking = 132.6°; Table 3). Therefore, in this work, we have the possibility of investigating the crystal structure of the HP$C2/c$ phase as a function of pressure. At the same time, we can reliably analyze changes in elasticity between the low- and high-pressure phases because the transformation occurs exactly at an intermediate pressure value between room pressure and the maximum pressure reached in this work (i.e., 8.7 GPa). The linear axial compressibility is obtained as $\beta_l = [(l - l_0)/l_0]/\Delta P$, where l and l_0 are the values of the cell parameter at a given pressure and room pressure and P is the pressure. For the unit-cell parameters of the low-pressure low-symmetry form, the axial compressibilities are –0.00311, –0.00313, –0.00348, and –0.00263 GPa^{-1} for *a*, *b*, *c* and $a\sin\beta$, respectively, with a compressibility anisotropy ratio of 1.18:1.19:1.32:1.00. An analogous calculation was done for the high-pressure high-symmetry form and gave: –0.00270, –0.00209, –0.00261, and –0.00215 GPa^{-1} for *a*, *b*, *c* and $a\sin\beta$, respectively, with markedly lower compressibility values with respect to those of the low-symmetry phase and an anisotropy ratio of 1.29:1.00:1.25:1.03. The differences in axial compressibility obviously affect the bulk volume compressibility, β_V, which is –0.00913 and –0.00680 GPa^{-1} for the low- and high-symmetry phases, respectively, indicating that the high-symmetry phase is about 34% more rigid than the low-symmetry one. Although the unit-cell volume-pressure data collected in this work are relatively limited, a second-order Birch-Murnaghan equation of state (BM2 EoS, Birch 1947) was used to fit the data and calculate the bulk modulus for the two $LiFeGe_2O_6$ phases. We obtained a K_{T0} of 100(4) GPa for the $P2_1/c$ phase and 132(9) GPa for the $C2/c$

[1] Deposit item AM-09-016, CIF. Deposit items are available two ways: For a paper copy contact the Business Office of the Mineralogical Society of America (see inside front cover of recent issue) for price information. For an electronic copy visit the MSA web site at http://www.minsocam.org, go to the American Mineralogist Contents, find the table of contents for the specific volume/issue wanted, and then click on the deposit link there.

TABLE 1. Summary of crystal data and structure refinements at high pressure

P (GPa)	0.00	1.25	2.54	4.16	4.83*	6.04	6.48*	8.72
a (Å)	9.893(1)	9.843(4)	9.801(4)	9.765(4)	9.500(9)	9.457(4)	9.448(9)	9.400(4)
b (Å)	8.836(6)	8.794(4)	8.769(5)	8.721(5)	8.711(8)	8.690(9)	8.670(8)	8.640(8)
c (Å)	5.379(5)	5.352(3)	5.331(4)	5.301(4)	5.127(6)	5.113(8)	5.101(8)	5.075(8)
β (°)	108.83(5)	108.70(5)	108.66(5)	108.49(5)	101.55(9)	101.41(9)	101.19(9)	100.92(9)
V (Å^3)	445.0(5)	438.8(4)	434.1(4)	428.1(4)	415.7(7)	411.9(8)	409.9(8)	404.7(8)
Space group	$P2_1/c$	$P2_1/c$	$P2_1/c$	$P2_1/c$	$C2/c$	$C2/c$	$C2/c$	$C2/c$
Z	4	4	4	4	4	4	4	4
θ_{max} (°)	29.85	29.49	29.63	29.77	29.16	29.26	29.35	28.90
Un. refl.	548	542	532	530	247	247	244	242
R_{int}	0.0716	0.0633	0.0971	0.0970	0.0814	0.0875	0.0695	0.0653
*R*1	0.0786	0.0643	0.1070	0.1075	0.0888	0.0763	0.0760	0.0805
GooF	1.060	1.120	1.213	1.157	1.125	1.289	1.104	1.130

* Data measured under decompression.

phase. Even though the standard deviations are relatively large (as expected from the limited data set), the difference between the two bulk moduli is significant and indicates that the *C*2/*c* phase is about 24% more rigid than the *P*2$_1$/*c* one. To explain such a significant difference for the *P*2$_1$/*c* and *C*2/*c* phases of $LiFeGe_2O_6$, a detailed analysis of the crystal structure evolution as a function of pressure is presented in the next section.

Crystal structure evolution

The clinopyroxene crystal structure is well known and is made up of three distinct types of oxygen-coordinated crystallographic sites: M1, M2, and T. In our sample, these sites are occupied by Fe, Li, and Ge, respectively. Both the M1 and M2 sites are coordinated by six O atoms, but the M2 site is more irregular and larger than the octahedrally coordinated M1 site. Cation polyhedra containing the M1 site form a zig-zag chain along the **c** axis. The M1 and M2 polyhedra are linked to the TO_4 tetrahedra forming an infinite chain along the **c** axis. In *C*2/*c* pyroxenes, one unique tetrahedral chain is present, while *P*2$_1$/*c* pyroxenes contain two symmetrically non-equivalent tetrahedral chains (A and B) and, hence, also two non-equivalent T sites (TA and TB). The A chain is more extended and the B chain is markedly more kinked, where the chain kinking angle is defined by the O3-O3-O3 bridging O atoms (Fig. 2).

Figure 3 shows the evolution of M2 and M1 polyhedral volumes as a function of pressure. These polyhedra do not show any significant discontinuity at the phase transition and decrease in volume with pressure by –12.5 and –6.3%, respectively. Such variations can be quantified by calculating the polyhedral volume bulk modulus following the same fitting procedure as the one used for the unit-cell volume-pressure data. Therefore a BM2 EoS was used to fit the M2 and M1 polyhedral volumes at the different pressures, yielding a K_{T0} of 59(6) and 135(17) GPa for M2 and M1 volumes, respectively, with M2 being distinctly more compressible than M1. The tetrahedral volumes in both *P*2$_1$/*c* and *C*2/*c* are nearly incompressible over the pressure range investigated, as expected for tetrahedra even if occupied by Ge (e.g., Hattori et al. 2000). Although the polyhedral volumes do not show discontinuities at the transition, an analysis of the geometrical distortion of polyhedra [calculated as $(V_i - V_p)/V_i$ where V_i is the volume of the ideal polyhedron, and V_p the volume of the coordination polyhedron, see Balić-Žunić and Vicković 1996] could provide information on the high-pressure deformation mechanisms. In Figure 4 and Table 3, the M2 and M1 polyhedral distortions are reported as a function of pressure. From Figure 4, it is possible to note that at the transition pressure a strong discontinuous decrease occurs for the M2 volume, whereas a small but significant change in slope characterizes the behavior of the M1 volume. In both *P*2$_1$/*c* and HP*C*2/*c* symmetries, we observe an increase of regularity with pressure; however, whereas the M2 trend persists into the *C*2/*c* phase stability field, the regularity of M1 polyhedra plateaus at the point of phase transition. To better explain the evolution of the polyhedral volumes and distortion parameters with pressure, the behavior of individual bonds needs to be analyzed. In Figure 5, the evolution of the M2-O bond lengths is shown with pressure. For the *P*2$_1$/*c* symmetry, the M2 polyhedron is characterized by six independent

Table 2. Atomic coordinates ($\times 10^{-4}$) and equivalent (only for Fe and Ge sites) and isotropic displacement parameters ($Å^2 \times 10^{-3}$) at high pressures

Atom	*x*	*y*	*z*	$U_{iso/eq}$
P = 0.00 GPa				
LiM2	2580(40)	200(50)	2200(50)	18(7)
FeM1	2510(3)	6500(4)	2153(5)	16(1)
GeA	453(2)	3420(3)	2797(4)	16(1)
O1A	8612(17)	3323(16)	1740(20)	16(3)
O2A	1082(18)	5178(17)	2850(20)	22(3)
O3A	1187(17)	2895(18)	6170(20)	19(3)
GeB	5517(2)	8394(3)	2311(4)	15(1)
O1B	3611(17)	8285(15)	1000(20)	16(3)
O2B	6311(18)	10039(16)	3850(20)	23(3)
O3B	6131(18)	6924(17)	4620(30)	23(3)
P = 1.25 GPa				
LiM2	2600(40)	130(50)	2210(60)	24(7)
FeM1	2505(3)	6509(3)	2128(5)	18(1)
GeA	457(2)	3420(3)	2811(3)	19(1)
O1A	8595(15)	3330(15)	1770(20)	17(3)
O2A	1121(16)	5201(17)	2840(20)	26(3)
O3A	1180(16)	2902(16)	6200(20)	19(3)
GeB	5530(2)	8394(3)	2300(3)	18(1)
O1B	3640(15)	8293(14)	1030(20)	19(3)
O2B	6294(17)	10050(17)	3860(20)	29(3)
O3B	6146(17)	6905(17)	4600(30)	24(3)
P = 2.54 GPa				
LiM2	2570(50)	134(66)	2309(80)	19(1)
FeM1	2508(4)	6508(4)	2110(6)	18(1)
GeA	455(3)	3422(3)	2830(5)	19(1)
O1A	8620(20)	3360(20)	1830(30)	22(4)
O2A	1150(20)	5200(20)	2880(30)	28(4)
O3A	1179(19)	2940(20)	6250(30)	14(3)
GeB	5536(3)	8392(3)	2298(5)	18(1)
O1B	3670(20)	8291(19)	1020(30)	17(4)
O2B	6290(20)	10040(20)	3890(30)	24(4)
O3B	6110(20)	6870(20)	4550(30)	25(4)
P = 4.16 GPa				
LiM2	2590(50)	140(60)	2410(80)	30(11)
FeM1	2516(4)	6508(4)	2092(6)	16(1)
GeA	457(3)	3424(3)	2848(5)	18(1)
O1A	8640(20)	3352(18)	1880(30)	17(4)
O2A	1140(20)	5230(20)	2890(30)	30(4)
O3A	1202(19)	2950(20)	6270(30)	18(4)
GeB	5546(3)	8388(3)	2299(5)	18(1)
O1B	3655(18)	8269(17)	960(30)	12(3)
O2B	6280(20)	10080(20)	3910(30)	24(4)
O3B	6110(20)	6810(20)	4520(30)	28(4)
**P* = 4.83 GPa				
LiM2	0	2710(50)	2500	18(8)
FeM1	0	9004(4)	2500	21(1)
Ge	3014(2)	929(2)	2164(4)	21(1)
O1	1119(16)	814(14)	1310(30)	20(3)
O2	3795(18)	2538(18)	3750(20)	28(3)
O3	3603(18)	646(18)	9180(30)	29(3)
P = 6.04 GPa				
LiM2	0	2760(50)	2500	16(8)
FeM1	0	9010(4)	2500	19(1)
Ge	3016(2)	934(2)	2163(4)	19(1)
O1	1145(14)	834(12)	1330(20)	12(3)
O2	3766(16)	2538(16)	3750(20)	22(3)
O3	3598(17)	675(16)	9130(30)	23(3)
**P* = 6.48 GPa				
LiM2	0	2761(40)	2500	11(7)
FeM1	0	9009(4)	2500	21(1)
Ge	3019(2)	934(2)	2163(4)	22(1)
O1	1116(15)	835(13)	1290(20)	19(3)
O2	3770(16)	2528(17)	3760(20)	28(3)
O3	3611(18)	679(17)	9170(30)	32(3)
P = 8.72 GPa				
LiM2	0	2700(50)	2500	17(8)
FeM1	0	9014(4)	2500	21(1)
Ge	3025(2)	935(2)	2163(4)	21(1)
O1	1120(16)	835(14)	1260(30)	22(3)
O2	3782(17)	2550(17)	3790(20)	26(3)
O3	3610(18)	684(17)	9120(30)	30(3)

* Data measured under decompression.

TABLE 3. Selected bond lengths (Å), polyhedral volumes (Å^3), polyhedral distortions, and angles (°) for $LiFeGe_2O_6$

P (GPa)	0.00	1.25	2.54	4.16		*4.83	6.04	*6.48	8.72
M2-O2B	2.063(31)	2.041(31)	1.982(42)	1.922(40)	M2-O2 × 2	2.043(14)	2.054(14)	2.048(13)	2.021(14)
M2-O3A$_{short}$	2.132(40)	2.181(40)	2.130(56)	2.111(54)	M2-O1 × 2	2.119(37)	2.142(35)	2.129(30)	2.086(35)
M2-O1B	2.178(40)	2.114(40)	2.173(56)	2.200(52)	M2-O3 × 2	2.239(32)	2.177(29)	2.170(26)	2.177(30)
M2-O1A	2.214(41)	2.144(38)	2.082(57)	2.074(54)	<M2-O>	2.133	2.124	2.116	2.095
M2-O2A	2.355(31)	2.343(31)	2.344(44)	2.387(41)	V_{M2}	12.65(22)	12.47(22)	12.30(18)	12.02(21)
M2-O3B	2.390(39)	2.380(38)	2.407(54)	2.367(53)	Volume distortion	0.0346	0.0285	0.0305	0.0281
<M2-O>	2.222	2.201	2.186	2.177					
V_{M2}	13.52(41)	13.22(42)	12.96(53)	12.66(50)	M1-O2 × 2	1.909(16)	1.924(14)	1.924(14)	1.904(15)
Volume distortion	0.0614	0.0583	0.0505	0.0485	M1-O1 × 2	2.034(14)	2.046(12)	2.019(13)	2.001(14)
					M1-O1 × 2	2.061(14)	2.073(12)	2.062(12)	2.057(14)
M1-O2B	1.930(15)	1.930(15)	1.932(19)	1.900(19)	<M1-O>	2.002	2.015	2.002	1.987
M1-O2A	1.960(15)	1.912(14)	1.899(20)	1.894(20)	V_{M1}	10.52(5)	10.75(6)	10.53(6)	10.30(5)
M1-O1B	2.012(13)	2.036(12)	2.038(16)	2.008(14)	Volume distortion	0.0101	0.0075	0.0100	0.0094
M1-O1A	2.035(13)	2.024(12)	2.040(17)	2.053(14)					
M1-O1B	2.120(14)	2.116(13)	2.122(17)	2.093(16)	T-O2	1.713(15)	1.696(14)	1.689(14)	1.707(14)
M1-O1A	2.147(14)	2.120(13)	2.140(18)	2.132(17)	T-O1	1.768(15)	1.738(13)	1.768(14)	1.764(15)
<M1-O>	2.034	2.023	2.028	2.013	T-O3	1.741(16)	1.746(14)	1.759(16)	1.743(16)
V_{M1}	10.95(6)	10.80(5)	10.92(6)	10.66(6)	T-O3	1.748(16)	1.760(15)	1.739(16)	1.748(16)
Volume distortion	0.0147	0.0136	0.0110	0.0111	<T-O>	1.743	1.735	1.739	1.741
					V_T	2.69(2)	2.66(2)	2.68(2)	2.68(2)
TA-O2A	1.670(15)	1.695(15)	1.698(19)	1.708(20)	Volume distortion	0.0084	0.0045	0.0059	0.0073
TA-O1A	1.726(16)	1.738(14)	1.705(22)	1.685(19)					
TA-O3A	1.747(15)	1.730(13)	1.738(17)	1.747(18)	Chain kink	132.6(5)	130.7(4)	130.5(6)	130.1(5)
TA-O3A	1.784(13)	1.782(12)	1.783(15)	1.776(15)					
<TA-O>	1.732	1.737	1.731	1.729					
V_{TA}	2.64(2)	2.66(2)	2.63(2)	2.61(2)					
Volume distortion	0.0086	0.0079	0.0086	0.0096					
TB-O2B	1.731(15)	1.726(15)	1.718(18)	1.741(18)					
TB-O3B	1.764(14)	1.757(13)	1.744(18)	1.737(18)					
TB-O3B	1.764(15)	1.766(14)	1.763(19)	1.781(19)					
TB-O1B	1.790(16)	1.766(15)	1.738(20)	1.759(17)					
<TB-O>	1.762	1.754	1.741	1.755					
V_{TB}	2.78(3)	2.75(2)	2.69(3)	2.75(3)					
Polyhedron distortion	0.0098	0.0064	0.0070	0.0098					
A chain kink	209.1(8)	209.6(9)	212.0(8)	213.0(8)					
B chain kink	138.5(6)	137.3(7)	135.3(8)	131.1(5)					

Note: Polyhedral volumes, polyhedral distortions, and relative errors were calculated using IVTON software (Balić-Žunić and Vicković 1996).
* Data measured under decompression.

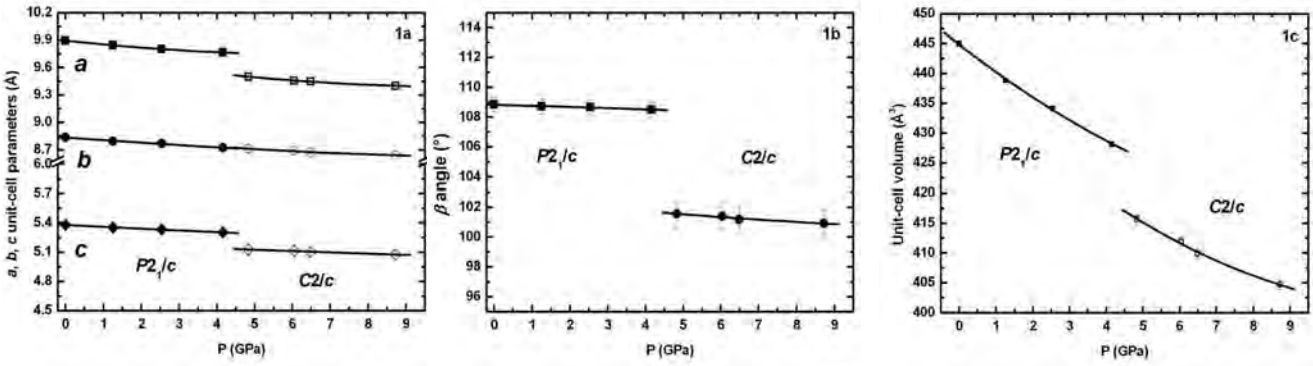

FIGURE 1. Evolution of the unit-cell parameters and unit-cell volume as a function of pressure for $LiFeGe_2O_6$ pyroxene. Variations in *a*, *b*, and *c* are shown in **a**; β and *V* in **b** and **c**, respectively.

distances, which become three pairs in the *C*2/*c* symmetry after the transition. Up to 4.16 GPa, before the transition, the largest decrease with pressure is shown by the M2-O2B and M2-O1A distances, which change by 7.3 and 6.8%, respectively, whereas all the other four distances show variations within about 1% (Table 3). From 4.89 to 8.72 GPa in the *C*2/*c* phase, the M2-O1 and M2-O2 distances, corresponding to M2-O2B and M2-O1A in the *P*2$_1$/*c* structure (Fig. 2), decrease by about 1.1 and 1.6%, respectively, whereas the third one, M2-O3, decreases by about 2.8%. Therefore, in general, we can observe that above the transition pressure the M2-O bond lengths become more rigid. An important aspect characterizing the phase transition is the behavior of the M2-O3A$_{long}$ distance. This distance is 3.714 Å below the transition pressure, which implies that the O3A atom is not in the coordination sphere of the M2 cation in the *P*2$_1$/*c* structure (Fig. 2). However, at the transition, the A tetrahedral chain undergoes extremely strong kinking allowing a shortening of the M2-O3A$_{long}$ distance from 3.714 to 2.238 Å and allowing the O3A$_{long}$ atom to enter the M2 coordination sphere with a total position shift of about 1.48 Å in just 0.67 GPa. As

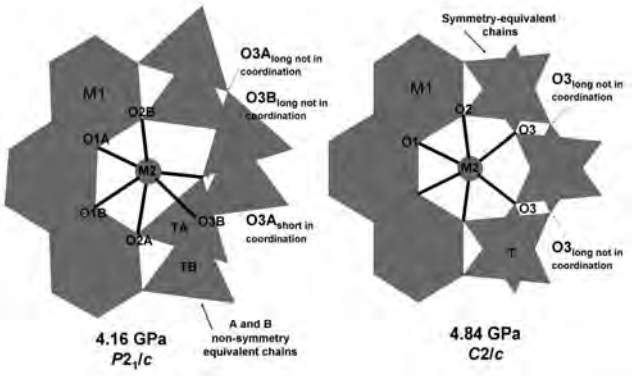

FIGURE 2. The crystal structure of $LiFeGe_2O_6$ pyroxene projected on the **bc** plane below (left side) and above (right side) the $P2_1/c$–$C2/c$ phase transition. In the $P2_1/c$ phase (left side), the two tetrahedral chains are not symmetry-equivalent.

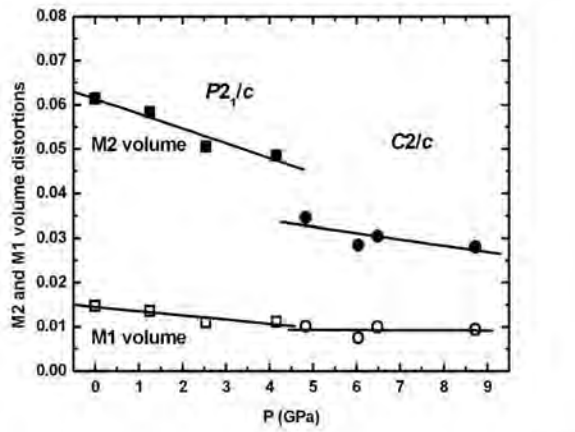

FIGURE 4. Evolution with pressure of M2 and M1 polyhedral distortions for $LiFeGe_2O_6$ pyroxene.

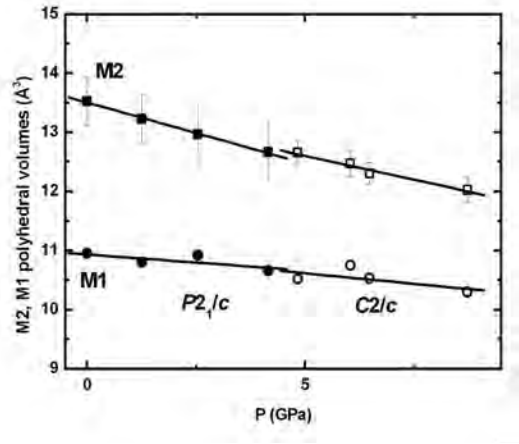

FIGURE 3. Evolution with pressure of M2 and M1 polyhedral volumes for $LiFeGe_2O_6$ pyroxene.

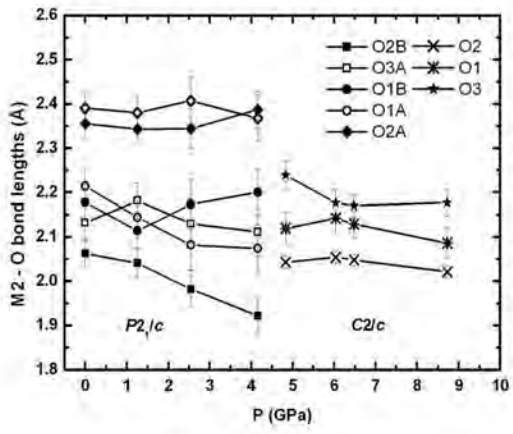

FIGURE 5. Evolution of M2-O bond lengths as a function of pressure for $LiFeGe_2O_6$ pyroxene.

a consequence of the strong kinking, the M2-$O3A_{short}$ distance undergoes a lengthening of about 0.7 Å from 2.112 (Table 3) to 2.800 Å, with the $O3A_{short}$ atom going out of coordination (Fig. 2). This extremely large structure adjustment makes the M2 cavity much smaller and very resistant to further compression above the transition. In fact, this is noticeable by the M2-O bond lengths in the *C*2/*c* form, which decrease very little with pressure in comparison with the changes in M2-O bond lengths with pressure in the $P2_1/c$ form.

In general, the M1 octahedron shows great rigidity, as also indicated by the evolution of the M1-O bond lengths. The average <M1-O> bond length decreases by just 1% below the transition and even less (0.75%) above the transition. Therefore, the M1 site practically behaves as a rigid unit for the examined clinopyroxene. Even less compressible are the tetrahedral volumes, with the average <T-O> bond length practically unchanged within the experimental errors throughout the pressure range investigated.

A crucial role in the high-pressure deformation mechanism is played by the O3-O3-O3 angle, which defines the kinking of a tetrahedral chain. From Table 3 and Figure 6, we can observe that in the $P2_1/c$ phase the A chain (S-rotated) extends with pressure by about 1.9% (~0.9°/GPa), while the B chain (O-rotated) kinks by about 5.3% (~1.8°/GPa). At the transition, the two A and B non-symmetry equivalent tetrahedral chains become equivalent showing an O-rotated configuration, and within the *C*2/*c* field they kink by just about 1.9%. Therefore, comparison of the total deformation of the two tetrahedral chains in the $P2_1/c$ structure with the evolution of the tetrahedral rotation above the transition shows that the tetrahedral chain in the HP*C*2/*c* phase is much more rigid.

DISCUSSION AND CONCLUDING REMARKS

In this study, we have investigated a sample of germanate clinopyroxene $LiFeGe_2O_6$ (space group $P2_1/c$ at ambient conditions) up to 8.7 GPa by single-crystal X-ray diffraction using a diamond-anvil cell. The sample shows a strongly first-order phase transition between 4.16 and 4.83 GPa as indicated by the strong drop in the *a*, *c*, β, and in the unit-cell volume. The *C*-centering of the lattice is clearly marked by the disappearance

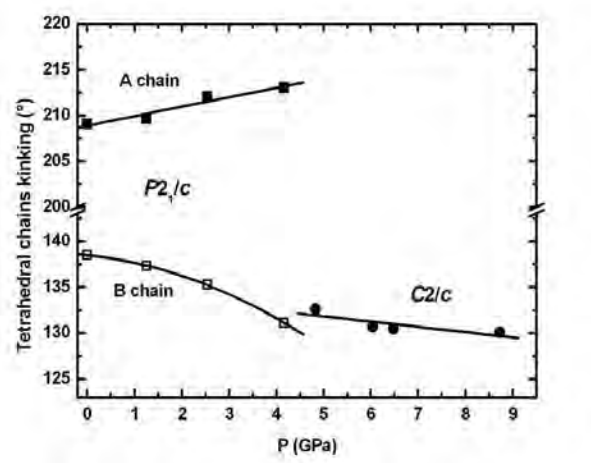

FIGURE 6. Evolution of the tetrahedral chains with pressure for $LiFeGe_2O_6$ pyroxene.

of *b*-type reflections ($h + k$ = odd) at the transition. The volume bulk modulus of the $P2_1/c$ phase was calculated to be 100 GPa as opposed to 132 GPa of the $C2/c$ one, with a difference in compressibility between the low- and high-symmetry phases of about 24%. Based on these results, the high-symmetry phase of $LiFeGe_2O_6$ represents the most rigid phase among the Li and germanate clinopyroxenes studied so far (e.g., Arlt and Angel 2000; Hattori et al. 2000; Gatta et al. 2005; Nestola et al. 2008). The only studies on a $P2_1/c$ clinopyroxene showing that the $C2/c$ phase is more rigid than the $P2_1/c$ phase are Nestola et al. (2004) and a work in preparation on natural pigeonite (BTS, Alvaro et al. unpublished). In conclusion, it appears that for clinopyroxenes the HP$C2/c$ phase is always more rigid than the $P2_1/c$ phase. It is clear that such an important difference must be taken into account in every geodynamic model involving the upper mantle, where pyroxenes represent around 20% by volume (e.g., Anderson 1989). In fact, thermodynamic calculations performed on the lower part of the upper mantle should be based on compressibility and thermal expansion determined for the high-pressure symmetry, which is stable at these depths. The reasons for the strongly different bulk moduli between the low- and high-symmetry phases must be examined in the context of crystal structure evolution with pressure.

The most remarkable crystallographic feature at the phase transition is the tetrahedral chain kinking: the A and B chains undergo strong deformations between 4.16 and 4.83 GPa (Fig. 2) with the consequence that the $O3A_{long}$ oxygen enters the M2 coordination, whereas the $O3A_{short}$ oxygen goes out. As a consequence, the M2 site is still sixfold coordinated in the HP$C2/c$ phase, but the cavity is strongly reduced in size and more regular (Fig. 2). Between 4.83 and 8.72 GPa, the $C2/c$ phase does not show strong deformation as the tetrahedral chain is extremely kinked and does not allow further significant deformation, at least within the investigated pressure range. This topology makes the high-pressure phase more rigid than the $P2_1/c$ one and at the same time accounts for the strong reduction in compressibility along the *b* and *c* axes by 33 and 25%, respectively, going from the $P2_1/c$ to the $C2/c$ phase, making the $C2/c$ phase slightly less anisotropic than the low-symmetry one.

ACKNOWLEDGMENTS

Financial support for this work was provided by MIUR-Rome to Alberto Dal Negro (PRIN 2006047943) and by the FWF-Vienna to G.J. Redhammer (P19762-N10). Two anonymous referees and Associate Editor A. Chakhmouradian are acknowledged for their reviews that allowed to definitively improve the manuscript.

REFERENCES CITED

Anderson, D.L. (1989) Theory of the Earth, p. 147–177. Blackwell Scientific Publications, Boston.

Angel, R.J. (2004) Absorption corrections for diamond-anvil pressure cells implemented in the software package—*Absorb6.0*. Journal of Applied Crystallography, 37, 486–492.

Angel, R.J., Chopelas, A., and Ross, N.L. (1992) Stability of high-density clinoenstatite at upper-mantle pressures. Nature, 358, 322–324.

Angel, R.J., Bujak, M., Zhao, J., Gatta, G.D., and Jacobsen, S.D. (2007) Effective hydrostatic limits of pressure media for high-pressure crystallographic studies. Journal of Applied Crystallography, 40, 26–32.

Arlt, T. and Angel, R.J. (2000) Displacive phase transitions in *C*-centred clinopyroxenes: spodumene, $LiScSi_2O_6$ and $ZnSiO_3$. Physics and Chemistry of Minerals, 27, 719–731.

Balić-Žunić, T. and Vicković, I. (1996) IVTON—a program for the calculation of geometrical aspects of crystal structures and some crystal chemical applications. Journal of Applied Crystallography, 29, 305–306.

Birch, F. (1947) Finite elastic strain of cubic crystals. Physical Review, 71, 809–824

Downs, R.T. (2003) Topology of the pyroxenes as a function of temperature, pressure, and composition as determined from the procrystal electron density. American Mineralogist, 88, 556–566.

Gatta, G.D., Boffa Ballaran, T., and Iezzi, G. (2005) High-pressure X-ray and Raman study of a ferrian magnesian spodumene. Physics and Chemistry of Minerals, 32, 132–139.

Hattori, T., Nagai, T., Yamanaka, T., Werner, S., and Schulz, H. (2000) Single-crystal X-ray diffraction study of $FeGeO_3$ high-*P* clinopyroxene ($C2/c$) up to 8.2 GPa. American Mineralogist, 85, 1485–1491.

Mao, H.K., Xu, J., and Bell, P.M. (1986) Calibration of the ruby pressure gauge to 800 kbar under quasi-hydrostatic conditions. Journal of Geophysical Research, 91, 4673–4676.

Nestola, F., Tribaudino, M., and Ballaran, D.B. (2004) High-pressure behavior, transformation, and crystal structure of synthetic iron-free pigeonite. American Mineralogist, 89, 189–196.

Nestola, F., Boffa Ballaran, T., and Ohashi, H. (2008) The high-pressure $C2/c$–$P2_1/c$ phase transition along the $LiAlSi_2O_6$–$LiGaSi_2O_6$ solid solution. Physics and Chemistry of Minerals, 35, 477–484.

Pommier, C.J.S., Downs, R.T., Stimpfl, M., Redhammer, G.J., and Denton, M.B. (2005) Raman and X-ray investigations of $LiFeSi_2O_6$ pyroxene under pressure. Journal of Raman Spectroscopy, 36, 864–871.

Redhammer, G.J. and Roth, G. (2004) Structural changes upon the temperature dependent $C2/c \rightarrow P2_1/c$ phase transition in $LiMe^{3+}Si_2O_6$ clinopyroxenes, Me = Cr, Ga, Fe, V, Sc and In. Zeitschrift für Kristallographie, 219, 585–605.

Redhammer, G.J., Roth, G., Paulus, W., Andre, G., Lottermoser, W., Amthauer, G., Treutmann, W., and Koppelhuber-Bitschnau, B. (2001) The crystal and magnetic structure of Li-aegirine $LiFe^{3+}Si_2O_6$: a temperature-dependent study. Physics and Chemistry of Minerals, 28, 337–346.

Ross, N.L. and Navrotsky, A. (1988) Study of $MgGeO_3$ polymorphs (orthopyroxene, clinopyroxene, and ilmenite structures) by calorimetry, spectroscopy, and phase equilibria. American Mineralogist, 73, 1355–1365.

Sheldrick, G.M. (1997) SHELX-97, program for crystal structure analysis (release 97-2). University of Göttingen, Germany.

Thompson, R.M. and Downs, R.T. (2003) Model pyroxenes I: ideal pyroxene topologies. American Mineralogist, 88, 653–666.

MANUSCRIPT RECEIVED JULY 5, 2008
MANUSCRIPT ACCEPTED NOVEMBER 21, 2008
MANUSCRIPT HANDLED BY ANTON CHAKHMOURADIAN